Pergamon

PII: S0191-8141(96)00101-0

Journal of Structural Geology, Vol. 19, No. 6, pp. 861 to 874, 1997

0191-8141/97 $17.00 + 0.00

Time slicing, an image processing technique to visualize the temporal development of fabrics

RENÉE HEILBRONNER

Geological Institute and Department of Scientific Photography, University of Basel, Bernoullistr 32, CH-4056 Basel, Switzerland

and

MARCO HERWEGH

Geological Institute, University of Berne, Baltzerstr. 1, CH-3012 Berne, Switzerland

(*Received* 10 *April* 1996; *accepted in revised form* 14 *November* 1996)

Abstract—Thinking of a sequence of images (or of frames of a film) as a three-dimensional x–y–t stack with two length dimensions (x, y) parallel to the image plane and one time dimension (t) perpendicular to it, we propose to cut this stack parallel to the time axis, thus producing so-called time slices. On these time slices, the horizontal dimension is length: a straight line parallel to any direction in the x–y plane of the images. The vertical dimension is time. The one-dimensional movements of particles parallel to the plane of section can be observed as straight or curved time traces, depending on whether the displacement rates of the particles are constant or variable.

To demonstrate practical applications of this idea, we use three sets of images that were recorded in the course of see-through simple shear experiments on norcamphor: two stacks of polarization images and one stack consisting of c-axis orientation images. The stacks were cut parallel to the shear zone boundary. Techniques for the acquisition of the original image sequences, the steps of digital image preprocessing and the preparation of the time slices (x–t images) are described in detail. Problems associated with the temporal calibration, the derivation of true bulk strain and bulk strain rates, and the distinction of artefacts receive special attention. The influences of strain localization and grain boundary migration are discussed. On time slices of orientation images, the spatial evolution of texture domains, passive lattice rotation and lattice reorientations associated with nucelation can be distinguished. © 1997 Elsevier Science Ltd

INTRODUCTION

In a recent set of *in situ* deformation experiments, we studied the microfabric evolution of a norcamphor mylonite (Herwegh, 1996; Herwegh *et al.*, in press), and analysed the development of grain and grain boundary shapes and of crystallographic preferred orientations. For the determination of strain and strain localization, marker particles were used, as described in the literature (Jessell, 1986; Bons *et al.*, 1993; Park, 1994). At regular intervals (density depending on the speed of the deformation), c-axis orientation images were derived using the computer integrated polarization microscopy (CIP) described by Panozzo Heilbronner and Pauli (1993, 1994).

Here we want to draw attention to a rather simple but powerful technique by which video films or image stacks can be analysed. We call the technique *time slicing* (Panozzo Heilbronner and Herwegh, 1995) because we propose to cut an image stack along a plane that is parallel to the time axis, as explained below. The resulting images are called time slices and permit the analysis of displacements of marker particles, grain boundaries and lattice rotations as a function of time.

THE IMAGE STACKS

In general, image stacks are composed of ordered sets of x–y images. The latter may represent sections taken at various positions along the z-axis (x–y–z stack) or regular images taken at various times t (x–y–t stack). From an x–y–z stack, the three-dimensional solid may be reconstructed, as in the case of medical tomographic imagery. In contrast, an x–y–t stack may be animated to yield a film. The x–y–t stacks discussed in this paper are sequences of images which represent consecutive stages of a geometric development. For these stacks, image size is held constant; the camera is held fixed during image capture.

Three sets of images will be considered. The first consists of 53 colour slides of an intermediate temperature and high strain rate (IT–HS) experiment taken under crossed polarized conditions. The images were captured using a Nikon 35 mm camera and converted to digital images (on Photo CD) in a Kodak photographic laboratory. During image processing the colour stack was converted to monochrome. The second set is a sequence of 55 images of a high temperature and low strain rate (HT–LS) experiment taken under crossed polarized conditions. A Nikon DCS direct digital infrared camera

and a narrowband interference filter with a transmittance of 700 ± 5 nm were used, resulting in a set of monochromatic images. The third set is a stack of *c*-axis orientation images (COIs) derived from the same HT–LS experiment. Each of the 17 RGB colour images was obtained by the CIP method described elsewhere (Panozzo Heilbronner and Pauli, 1993). The first set will be referred to as IT–HS Pol, the second as HT–LS Pseudopol and the third as HT–LS COI.

THE TECHNIQUE OF TIME SLICING

Preparing a temporal sequence of images

Time slicing requires that the stack of images be perfectly matched. This condition is automatically fulfilled when recording the experiment with a stationary camera. However, in the course of long-lasting experiments, refocusing and change of cameras often induces shifts and misalignments which need to be corrected. Also, in the context of CIP analysis, 22 images have to be rematched for each orientation image. This in turn causes the sequence of orientation images to be slightly shifted with respect to one another. For this reason, the HT–LS COI stack required minor additional rematching. As a general practice, we used the image processing program NIH Image 1.57 (Rasband, 1995) to check the superposition of the images of any image stack by animating the stack.

In order to correlate microfabric changes with time correctly, the time lapse between the individual images of the stack must be constant. This is automatically achieved by recording the experiment at constant time intervals (or filming at a fixed number of frames per second) as was the case during the IT–HS experiments. However, in other circumstances, in particular if experiments span more than 1 day, the time lapses between images may vary as in the case of the HT–LS experiment (table 2 in Herwegh *et al.*, in press). In the case where images are missing empty frames may be inserted, as will be explained in the context of the HT–LS Pseudopol stack. In cases where the spacing is irregular, an appropriate scaling needs to be performed along the time axis.

For a stationary reference grain, the colour or grey value should remain constant throughout the image stack. In other words, lighting intensity, the orientation of the crossed polarizers or the orientation of the colour look-up table (CLUT) must remain the same for all images in the stack. If hue, saturation or brightness or the grey level of the reference grain change with time, the time slices are more difficult to interpret.

To enhance the visibility of N–S trending *c*-axes (N–S running parallel to the *y*-direction of the *x*–*y* images), the crossed polarizers and the lambda plate were rotated counterclockwise about an angle of 45° with respect to the standard orientation (Herwegh and Handy, 1996). For the optically negative norcamphor, this results in the yellow quadrants of the conoscopic image facing north and south (instead of northeast and southwest) and the blue quadrants east and west (instead of northwest and southeast). The black and white rendition of these colours assigns bright grey values to the yellow hues, intermediate grey values to the blue hues and dark grey values to first-order red.

The HT–LS Pseudopol stack consists of a series of monochrome infrared images. The spectral intensity distribution of the first order interference colours is such that when using an infrared transmission filter yellow appears brightest, blue darkest and first-order red as an intermediate grey. Note that this grey value rendition of interference colours is different from the one described for the IT–HS stacks. The colouring scheme of the HT–LS COI stack is given by the standard colour look-up table and remains constant throughout the stack.

Combining images to stacks

In the context of preprocessing, Adobe Photoshop 3.0.4 was used to convert the RGB orientation images to indexed colour. Next, NIH Image 1.57 was used to rematch the images. For the preparation of the time slices we used the stack menu of NIH Image 1.57. The images were loaded in the appropriate sequence and the windows were combined to a stack. At the site of missing images, empty images were inserted in the stack. The coordinate system pertaining to the stack configuration is shown in Fig. 1.

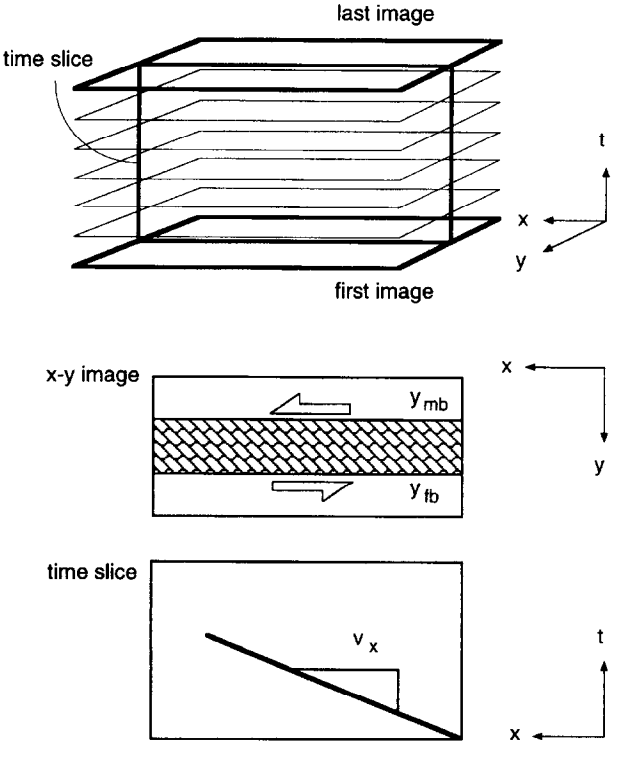

Fig. 1. Schematic representation of *x*–*y*–*t* image stack and time slices. Images represent the *x*–*y* planes of the stack; time slices correspond to *x*–*t* sections. Shear sense is sinistral. y_{mb} = *y*-pixel-coordinate of the upper, moving boundary of the shear zone, y_{fb} = *y*-pixel-coordinate of the lower, fixed boundary of the shear zone.

Using NIH Image 1.57, image stacks can only be cut vertically, that is parallel to the time direction. However, it is possible to choose any direction in the x–y plane. For the experiments considered here, we chose slices parallel to the shear plane, i.e. parallel to the applied displacement direction (x-direction). The x–y coordinate system of the images has x pointing to the left, y pointing down. The upper part of the section is moving to the left (sinistral shearing in the x–y plane) while the bottom part remains fixed. The shear zone is in the central part of the image; the shear zone boundaries run parallel to the x-direction.

Slicing

Each of the stacks discussed here was cut five times: twice in the 'wallrocks', i.e. within the undeformed region that is attached to the frosted grips (see fig. 1a in Herwegh and Handy, 1996), and three times within the deforming shear zone. The stacks were sliced 'vertically' (as shown in Fig. 1) by cutting the x–y–t image stack parallel to the x-direction and parallel to the time axis, setting the reslice option of NIH Image 1.57 to one pixel. This resulted in very narrow time slices since the t-dimension (resulting from the number of images) was on the order of 50 pixels or less while the x-dimension (which is the x-dimension of the stacked images) was usually on the order of several hundred pixels.

Thus, the time slices were stretched parallel to the time direction. Stretching requires bi-linear or bi-cubic interpolation. Although NIH image can slice black and white and colour stacks (provided they are indexed colour), it can only perform a bi-linear interpolation if the image is a grey value image. Thus, for the stretching of time slices of indexed colour stacks, Adobe Photoshop was used. If the time lapse between the images of a stack is large, i.e. if the displacements from one time increment to the next are large, the resulting time slices appear jagged and require additional smoothing. For this reason the time slices of the HT–LS COI stacks were smoothed before and after stretching. The loss of resolution is counterbalanced by the gain of 'readability'.

SCALING OF THE TIME SLICES

The x-dimension of the time slices is scaled by the same factor as the x–y images. Table 1 lists the x–y dimensions in pixels and the scaling factors. Scaling of the time dimension of the time slices depends on the time lapse and the stretching factor. The time lapse in the IT–HS experiment is 5 min, in the HT–LS Pseudopol 1 h and in the HT–LS COI 3 h. Stretching was eight times in all cases resulting in three different scaling factors which are also listed in Table 1. For the IT–HS Pol, the HT–LS Pseudopol, and the HT–LS COI, the x-units are 23.5 μm/pixel, 17.9 μm/pixel and 17.9 μm/pixel, the t-units are 37.5 s/pixel, 450 s/pixel and 1350 s/pixel, respectively.

When turning the time slices 90° in a clockwise sense (aligning the t-axis with the horizontal), we are faced with scaled $x(t)$ representations. On these rotated velocity graphs (Fig. 1), steep slopes represent high displacement rates.

INTERPRETATION OF THE TIME SLICES

As a first example we consider the time slices obtained from sectioning the IT–HS stack shown in Fig. 2 along the five traces indicated in the figure. On Fig. 3, these five time sections are shown, labelled according to the y-coordinate along which they were sectioned. The individual grains appear as stripes, running vertically or inclined, straight or curved, from the bottom to the top of the slices. The light and dark greys represent different crystallographic orientations. The boundaries between light and dark stripes are the time traces of the grain boundaries.

In accordance with the type of experiments analysed here, the discussion of the time slice interpretation is restricted to simple shear situations with sinistral shearing parallel to the horizontal x-direction of the x–y images (Fig. 1).

INTERMEDIATE TEMPERATURE–HIGH STRAIN RATE EXPERIMENTS: POLARIZATION IMAGES (IT–HS POL)

Recalculation of total shear strain and shear strain rate

In the high strain rate experiments, the velocity of the moving specimen grip was set to 0.0011 mm s^{-1}, resulting in an applied shear strain rate of 5.5×10^{-4} s^{-1} within the shear zone. On the time slice Y040 (upper left

Table 1. Dimensions of image stacks

Experiment	Image type	x pixel	y pixel	x-y scaling pixel/mm	no. of images	t pixel	t scaling pixel/hour
IT–HS Pol	RGB	616	229	42.5	53	424	96
HT–LS Pseudopol	grey	570	320	56	56	448	8
HT–LS COI	RGB	570	320	56	17	136	2.67

x, y: spatial dimension (width and height) of images.
t: time dimension of stack (height of time slices).

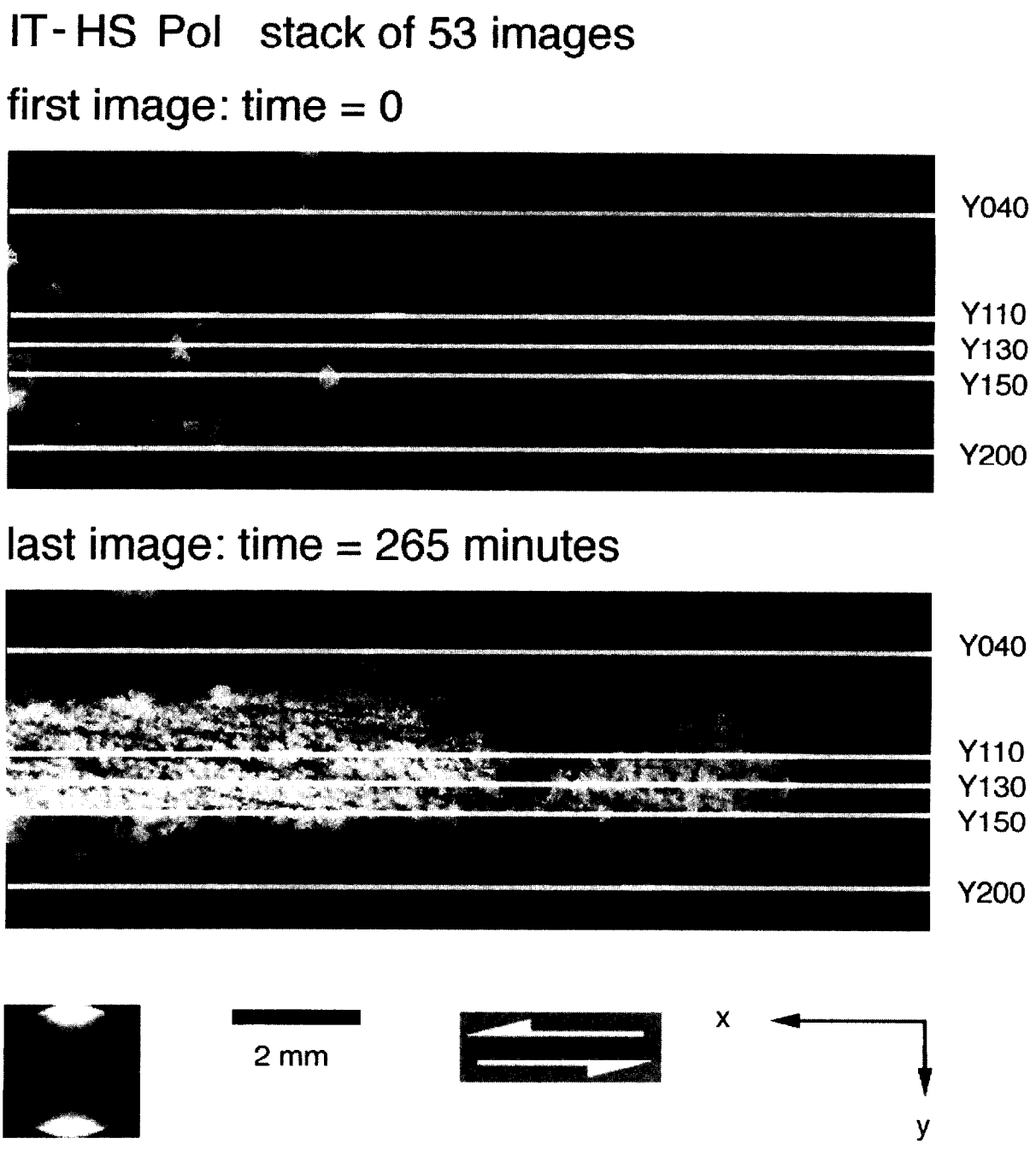

Fig. 2. First and last image of stack of IT–HS experiment on norcamphor (IT–HS = intermediate temperature, high strain rate). Images were taken with a 'Wild Photoautomat' camera. Traces for slicing at $y = 40$, 110, 130, 150 and 200 are indicated. Grey values correspond to crossed polarizer conditions (yellow = bright, magenta = dark, blue = intermediate grey). For details of experimental conditions and polarizer orientation, consult Herwegh *et al.* (in press). Inset: stereographic representation of the grey values.

in Fig. 3), the motion of the grip is seen as a constant slope of all grain boundary time traces. In some of the experiments, the bond between the glass plate and the norcamphor is not perfect, introducing a discrepancy between the x-displacement of the glass plate and that of the 'wallrock' material. For this reason, the 'true bulk shear strain rate' is re-calculated from the 'true bulk shear displacement' of the norcamphor, as follows.

The grain boundaries may be taken as passive markers of displacement. This is justified because in the intermediate temperature and/or high strain rate experiments, the amount of static or dynamic recrystallization of norcamphor in the 'wallrock' material may be neglected. Straight lines are fitted to the the grain boundary time traces of time slice Y040 (see white lines on Fig. 3), and the total x-displacement, Δ_x, is determined to be 652

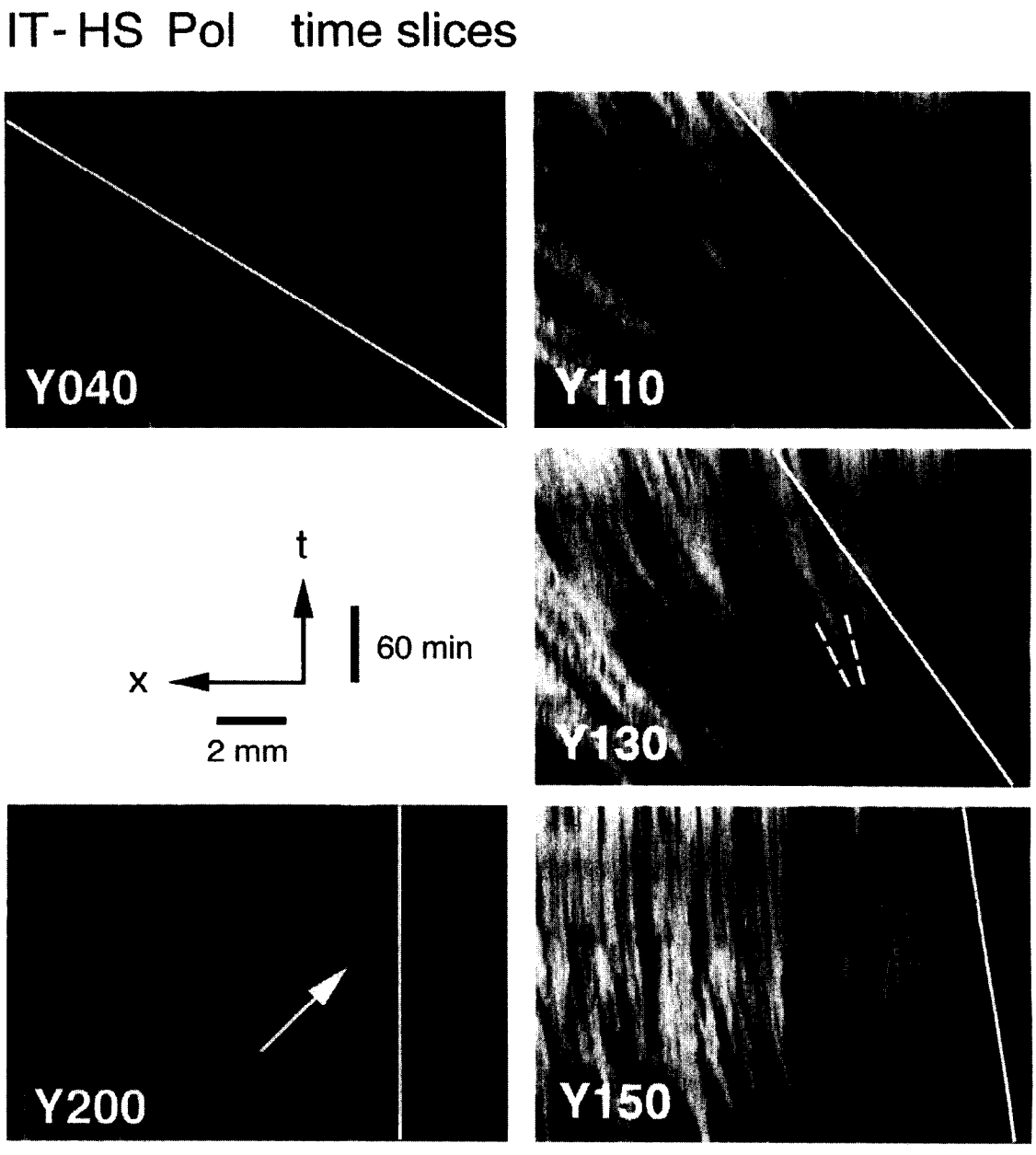

Fig. 3. Time slices of IT–HS-stack (Fig. 2). Slices at Y040 and Y200 are within the undeformed 'wallrock', slices Y110, Y130 and Y150 within the shear zone. Grey values correspond to crossed polarizer conditions (yellow = bright, magenta = dark, blue = intermediate grey). The solid white lines on the time slices represent x-displacement rates. For time slice Y040 the x-displacement rate, v_x, was recalculated from the bulk behaviour of the 'wallrock' material (see text for explanation). For time slices Y110, Y130 and Y150, the theoretical x-displacement rates, $v_x(y)$, were calculated from the x-displacement rate, v_x, of Y040 and the y-position of the time slice (see equation 4 in text). Dashed white lines indicate divergent grain boundaries, arrow points to coalescence of grains (see text for discussion).

pixels, i.e. 15.3 mm. Since the width of the shear zone (on the x–y plane) is 85 pixels, i.e. 2 mm, the resulting total shear strain, γ, is 7.7. Since the height of the time slice Y040 corresponds to 265 min, the true bulk shear strain rate is $4.82 \times 10^{-4}\ s^{-1}$ (Table 2). Note that the IT–HS experiment discussed here is not the same as listed in table 2 of Herwegh *et al.* (in press).

Differential shear displacement within the shear zone

Consider first the lower part of the x–y images representing the region of the stationary grip, i.e. the immobile 'wallrock'. The corresponding time slice Y200 (Fig. 3) shows the grain boundary time traces as approximately vertical parallel lines. The superposed vertical white line indicates that the x-displacement, Δ_x, is zero. Minor wiggles indicate insufficient image matching in the x-direction. Since these wiggles are parallel to one another, it is improbable that they should be caused by grain boundary migration. In the upper right of the image (arrow), it appears as if two bright grains merge at the expense of a dark one. This could be interpreted as an instance of grain consumption. However, in low temperature experiments the undeformed material of the

Table 2. Total shear strain and shear strain rate

Experiment	T_h	T (°C)	y_{mb} (pixels)	y_{fb} (pixels)	Δy	x-disp.	γ	t (min)	$\Delta\gamma/\Delta t$ (s^{-1})
IT-HS Pol	0.77	10	72	157	85	652	7.7	265	4.82×10^{-4}
HT–LS Pseudopol	0.81	25	88	228	140	1064	7.6	3240	3.91×10^{-5}
HT–LS COI									

T_h: (T/T_m) homologous temperature (T_m = 92–96°C).
y_{mb}: y-coordinate of moving shear zone boundary.
y_{fb}: y-coordinate of fixed shear zone boundary ($y_{mb} < y_{fb}$).
Δy: width of shear zone boundary in pixel.
x-disp.: total displacement of moving grip in the x-direction.
γ: total shear strain.
$\Delta\gamma/\Delta t$: average shear strain rate.

Table 3. x-displacement as function of y-coordinate

Experiment	Δx_{mb} pixels	Δx_1 pixels	Δx_2 pixels	Δx_3 pixels	Δt pixels
IT-HS Pol	652	361	207	54	424
HT-LS Pseudopol	1064	365	213	61	448
HT-LS COI	1064	365	213	61	136

Δx_{mb}: x-displacement of moving grip (= maximum displacement).
Δx_1: x-displacement at y = 110 (IT–HS) or y = 180 (HT–LS).
Δx_2: x-displacement at y = 130 (IT–HS) or y = 200 (HT–LS).
Δx_3: x-displacement at y = 150 (IT–HS) or y = 220 (HT–LS).
Δt: total time of experiment.

'wallrocks' did not recrystallize to any significant extent; at least, there is no change of average grain size, and again, the effect is attributed to poor image matching, this time in the y-direction.

Across the shear zone the x-displacement, Δ_x, decreases from 652 pixels to zero. Assuming homogeneous simple shear, the x-displacement within the shear zone is a linear function of y. At the upper shear zone boundary and within the 'wallrock' of the moving grip, where $y \geq y_{mb}$ (see Fig. 1), the total x-displacement, Δ_{xtot}, is 652 pixels. At the lower shear zone boundary and within the 'wallrock' of the fixed grip, where $y \leq y_{fb}$, the total x-displacement, Δx_0, is 0 pixels. The total width of the shear zone is Δy_{tot}

$$\Delta y_{tot} = |y_{mb} - y_{fb}|. \quad (1)$$

The total shear strain across the shear zone is γ

$$\gamma = \Delta x_{tot}/\Delta y_{tot}. \quad (2)$$

The x-displacement and the x-displacement rate at any given point within the shear zone are functions of y

$$\Delta x(y) = \gamma.|y_{fb} - y| \ (y_{mb} \leq y \leq y_{fb}) \quad (3)$$

$$v_x(y) = \Delta x(y)/\Delta t. \quad (4)$$

The total x-displacements for y = 110, 130 and 150 have been calculated and the appropriate x-displacement rates, v_x, are superposed on to the time slices (white lines in Fig. 3).

Deviations from simple shear

If the material within the shear zone had deformed homogeneously and by intracrystalline plasticity only, i.e. if there had been no grain growth nor any grain boundary migration, the grain boundaries would have acted as strain markers, tracing the geometry of deformation as one of homogeneous simple shear. On time slices, this would have resulted in straight and parallel grain boundary traces whose x/t slopes depend on the y-coordinate of the time slice, since the x-displacement, Δ_x, and the x-displacement rate v_x are linear functions of y, just as the white lines superposed on the time slices of Fig. 3. For time slices near the moving boundary of the shear zone, y_{mb}, the displacement rate, v_x—which is really $v_x(y)$—would be maximal, for time slices near y_{fb}, the displacement rate, v_x, would be zero, resulting in a zero slope on $x(t)$ plots, i.e. in vertical traces on the time slices (cf. also Table 3). For the experiments discussed here, however, it is obvious that the shape of the grain boundary time traces deviates from these 'ideal' tracks in various ways: the shear zone may rupture, macroscopic strain localization may occur, grain boundaries may start to migrate.

On time slice Y040 (Fig. 3), a large part of the shear zone material had moved out of the frame of the x–y image, leaving a dark triangle in the upper right which represents the magenta colour of the empty background. Rupture is seen on time slice Y110 and Y130, where straight grain boundary time traces turn abruptly into a vertical direction, indicating that a number of grains are

torn off from the deforming part of the shear zone material, remaining immobile with respect to the fixed glass plate from that time on.

The effect of strain localization and grain boundary migration

On time slices Y110, Y130 and Y150, the time traces of grain boundaries are not straight. At the very beginning of the experiment, i.e. near the bottom of the time slices, grain boundary time traces are parallel to one another and closely parallel to the theoretical v_x lines. As the displacement progresses, however, the grain boundary time traces deviate from the calculated v_x, and they diverge from one another. Below, we discuss these two types of deviation. (1) The deviation of the $x(t)$ slope of the otherwise parallel grain boundary time traces is attributed to macroscopic strain localization. Macroscopic strain localization refers to an area that encompasses a large number of grains and is explicitely distinguished from microscopic strain localization produced by intergranular shear zones. (2) The divergence of grain boundary time traces from one another is attributed to grain boundary migration.

(1) Strain localization and the associated deviations of the grain boundary time traces from the calculated v_x lines reflect the experimental boundary conditions. At the beginning of the experimental run, strain is localized at the diagonally opposed ends of the shear zone—'wallrock' interfaces. The sample area that is monitored by the x–y images shown here, is situated near the left side of the sample. Therefore, at the beginning, only the strain localization occurring in the lower left of the x–y images is visible. As the experiment progresses the upper right area of strain localization is moved into the picture (see fig. 4.8 in Herwegh, 1996). As a consequence, on time slice Y150, which is sectioned near the lower shear zone boundary (Fig. 3), the grain boundary time traces deviate from the v_x line. During the first stages of the experiment, i.e. near the bottom of the time slice, the slopes of the grain boundary time traces indicate higher velocities than the calculated v_x line. This effect is attributed to increased strain in this part of the shear zone. At later stages, the decreasing $x(t)$ slopes of the grain boundary time traces indicate that the zone of high strain intensity has moved out of the region which is sectioned by time slice Y150. Note that on time slice Y110, no 'accelerated' grain boundary time traces are visible, indicating that no macroscopic strain localization occurred in the corresponding region of the shear zone boundary.

(2) The divergence of grain boundary time traces is explained by grain growth via grain boundary migration. Principally, when observing the time slice by itself, the divergence could be explained in a number of ways. For example, one could claim that it is caused by components of displacement along microshears which are not parallel to the shear zone boundary, as observed by Herwegh and Handy (1996). However, direct observation of the x–y images of the shear zone reveals clearly that grain growth is pervasive at the given time steps and that the contributions of displacements parallel to microshears are so small as to be considered negligible.

The onset of grain growth is the t-coordinate where the grain boundary time traces start to diverge significantly from one another. In the case of the IT–HS experiments this appears to be within the first few increments of displacements, i.e. near the bottom of the time slice Y150. Comparing the time slices it appears that the onset of grain growth occurs at different points in time for different time slices. Obviously, the onset is not a function of time itself. But, whether it is a function of the accumulated strain or of the local strain rate could not be decided in this case.

Displacement of shear zone boundaries

In the middle of the t-dimension of time slice Y150 the grain boundary time traces become nearly vertical and parallel. From this point on, the time slice resembles that of the fixed 'wallrock' (Y200), differing from the latter only by a certain amount of recrystallization which is evidenced by a small number of tapering time sections. Following the explanation given in the section above, this could be attributed to strain localization occurring somewhere else in the sample, leaving the region of time slice Y150 undeformed.

Two alternative explanations will be given here. One is that the time section is not really situated within the shear zone but within the wallrock. In this case, at the beginning of the experiment, 'wallrock' material close to the shear zone would have been affected by the deformation of the shear zone, and the sharply defined boundary between shear zone and 'wallrock' would have been established only after a certain amount of deformation. The second possibility is inverse to this. Assuming that the time section is indeed situated within the shear zone, the width of the shear zone must change with time. In this case, in the course of the experiment, shear zone material would have attached itself to the stationary wallrock, and the shear zone boundary would have moved into the shear zone, thus narrowing the shear zone by a small amount. Unfortunately neither of these explanations can be tested rigorously, mainly because the boundary is not exactly parallel to x, possibly causing the section Y150 to crosscut the boundary.

HIGH TEMPERATURE–LOW STRAIN RATE EXPERIMENT: PSEUDO-POLARIZATION IMAGES (HT–LS PSEUDOPOL)

The images of the stack (Fig. 4) and the time slices (Fig. 5) are monochrome pictures taken with the Nikon DCS infrared camera, as described previously. The stack was

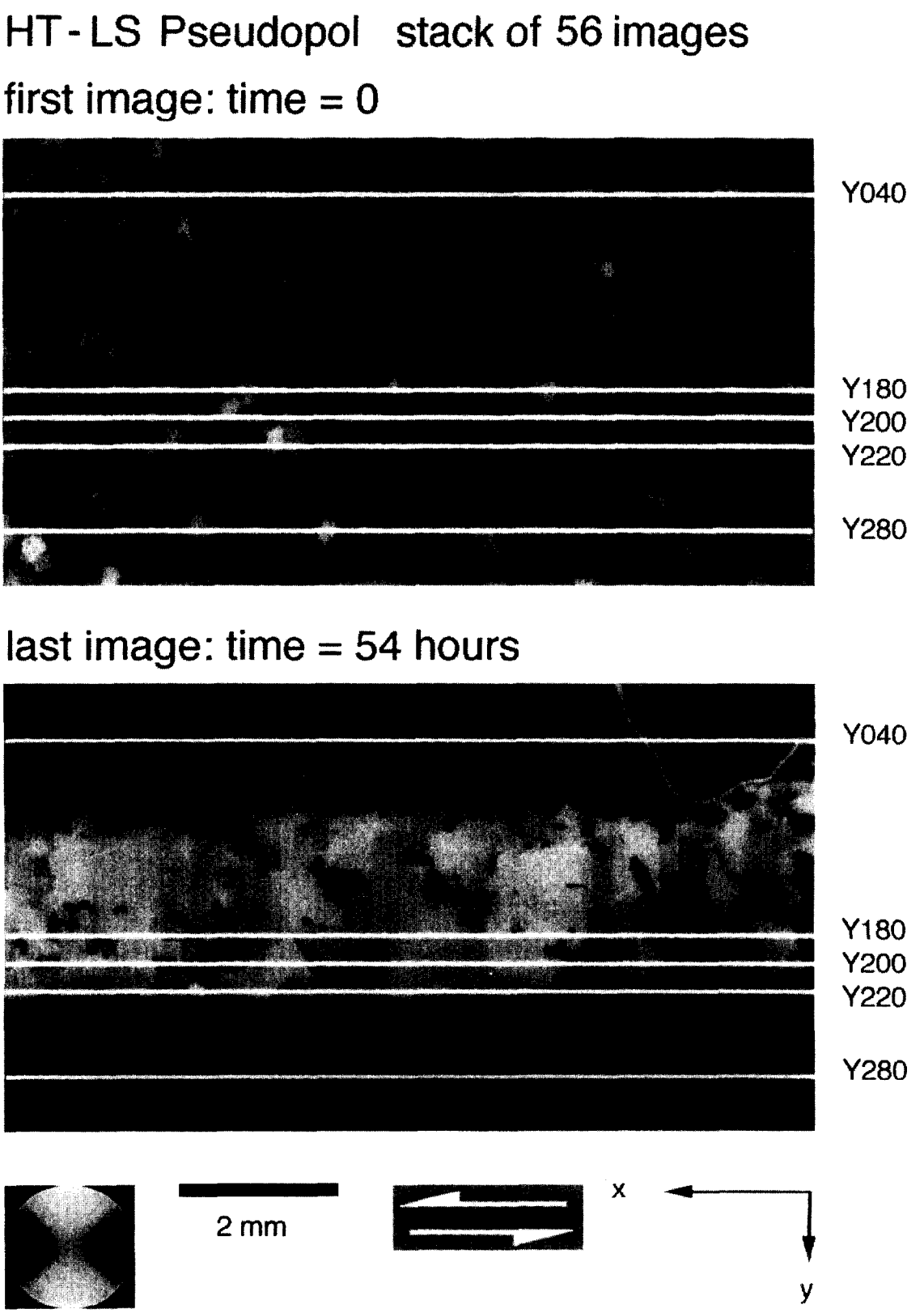

Fig. 4. First and last image of stack of HT–LS experiment on norcamphor (HT–LS = high temperature, low strain rate). Images were taken with direct digital camera. Traces for slicing at $y = 40$, 180, 200, 220 and 280 are indicated. Grey values correspond to crossed polarizer conditions recorded at $l = 700$ nm (yellow = bright, magenta = intermediate grey, blue = dark). For details of experimental conditions and polarizer orientation, consult Herwegh *et al.* (in press). Inset: stereographic representation of the grey values.

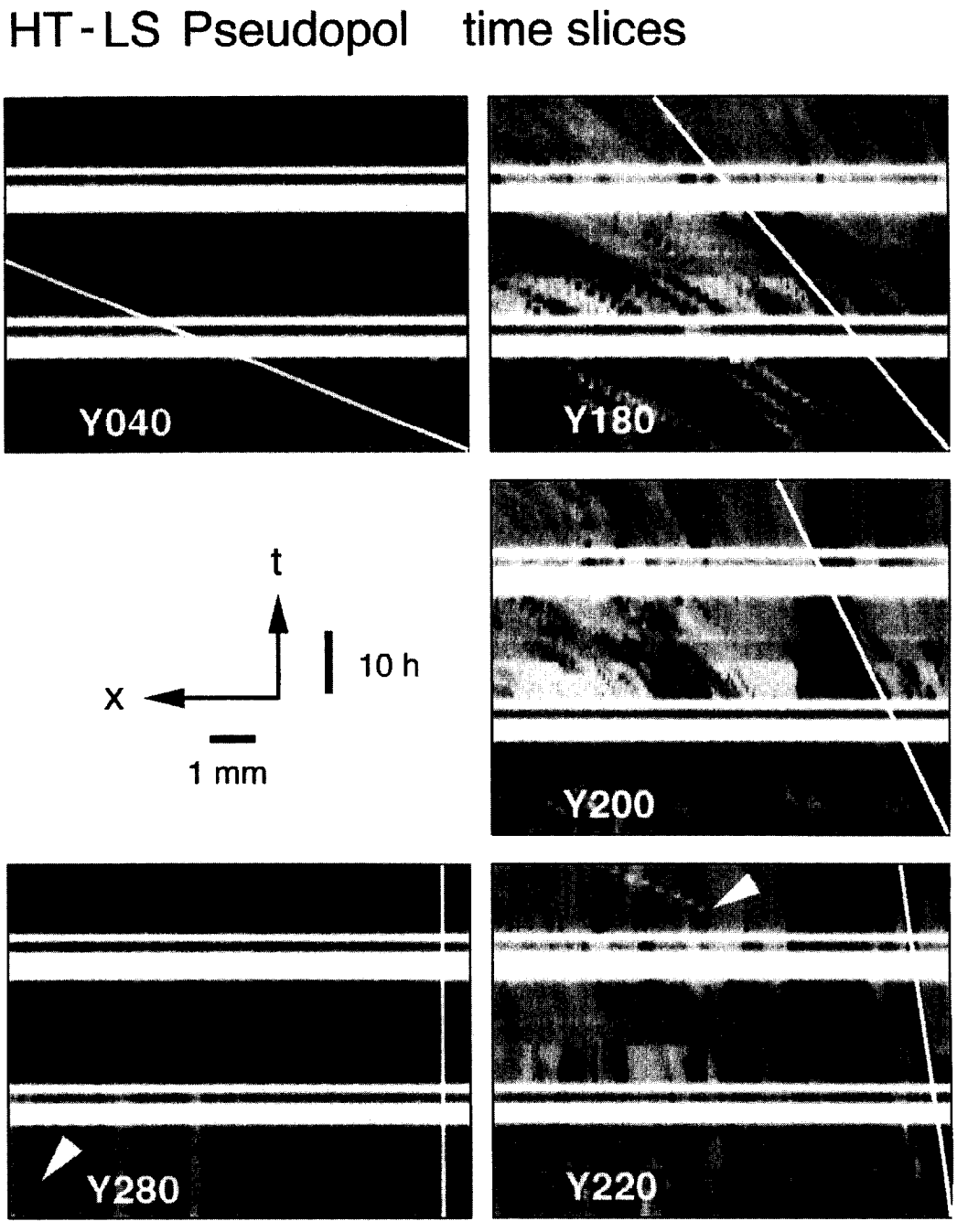

Fig. 5. Time slices of HT–LS-stack (Fig. 4). Slices Y040 and Y280 are within the undeformed 'wallrock', slices Y180, Y200 and Y220 within the shear zone. Grey values correspond to crossed polarizer conditions (yellow = bright, magenta = dark, blue = intermediate grey). Horizontal white stripes are due to empty frames which were inserted to scale the omissions in the recording sequence (see text for discussion). The solid white lines on the time slices represent x-displacement rates. For time slice Y040 the x-displacement rate, v_x, was recalculated from the bulk behaviour of the 'wallrock' material (see text for explanation). For times slices Y180, Y200 and Y220, the theoretical x-displacement rates, $v_x(y)$, were calculated from the x-displacement rate, v_x, of Y040 and the y-position of the time slice (see equation 4 in text). See text for explanation of abrupt changes of grey values at $t = 21$ h and 27 h. Arrows point to dust particles.

cut five times: twice within the 'wallrock', at $y = 40$ and $y = 280$, and three times within the shear zone at $y = 180$, $y = 200$ and $y = 220$.

Artefacts

The polarizer lambda plate assembly was re-oriented twice, changing from an orientation parallel to the x-direction to one of 30° clockwise rotation at $t = 168$ (corresponding to $t = 21$ h) and once again to one of 140° at $t = 216$ (corresponding to $t = 27$ h). The latter two orientations are roughly 90° from one another, their grey values more or less inverse. To achieve a better grey value match, the images of the last set (approximately the upper half of the time slice) were re-inverted (Fig. 5). As a consequence, opaque particles appear white instead of

black. For example, two relatively large dust particles (sitting on the glass cover presumably) can be tracked as a black stair step arrangement of dots in the lower left corner of time slice Y280, and as a white one near the upper border of time slice Y220 (arrows in Fig. 5).

The pictures of the high temperature–low strain rate experiment were taken over a period of 55 h at hourly intervals. During the night a number of pictures were omitted. In order to retain a constant scaling along the t-dimension, the equivalent number of empty images were inserted in the stack. In this manner, the Time Traveller's condition for the continued existence of the experiment was met (Wells, 1895), but unlike what one would expect from other recordings (Warhol, 1963), time slicing of sleep only produced strips of white canvas. . . .

Grain growth and grain boundary migration

In contrast to the previous example, there is significant grain growth, most obviously within the shear zone but also, to a lesser extent, within the wall rock. The latter is best seen in the upper half of the time slice Y280. Near the left and in the middle of the slice, two black grains can be observed whose diameter grows to more than twice their original size. Within the shear zone, grain growth is much more pronounced, yielding time sections with highly divergent grain boundary traces (see slice Y200).

The opening angle (between the grain boundary time traces) not only depends on the rate of grain growth but also on the y-coordinate of the time slice, i.e. on the inclination of the constant velocity lines (v_x). Thus, although the opening angle conveys some information concerning the rate of grain growth, it is not easy to use in the case where different time slices are to be compared.

Comparing the time traces of grain boundaries to the calculated displacement rates (straight white traces on Fig. 5), one notes that already within the first few increments, the sinistral movement of grain boundaries is faster than the theoretical x-displacement rate v_x. Again, this apparent 'sinistral acceleration' of grain boundaries is attributed to early strain localization (Herwegh, 1996). However, in contrast to the IT–HS experiment, this effect cannot only be seen at the very boundary of the shear zone (on time slice Y220) but also in the interior of the shear zone (on time slice Y180), indicating that the zone of strain localization is wider than in the previous case.

Although minor evidence of grain growth can be found in the very first increments of deformation, there appears to be a significant increase at a later stage. Significant grain growth occurs after one third of the experiment on time slice Y180, after only one sixth on Y200. These turnovers are hard to spot mainly because of the aforementioned change of polarizer orientation. Huge grain diameters are attained for bright grains (yellow grains in Herwegh *et al.*, in press), i.e. for grains that have the c-axes pointing in the y-direction of the x–y images (N on the stereogram). It appears that reaching this preferred crystallographic orientation and rapid grain growth are intimately related. Since this condition is dependent on strain (Herwegh, 1996), and since strain localization starts near the shear zone boundary, one can observe the onset of rapid grain growth moving with time from a region near the shear zone boundary (Y200) towards the centre of the shear zone (Y180).

Boundary effects

Slice Y220 is again very close to the shear zone boundary, and the considerations described for Y150 of the IT–HS experiment apply here too. In addition, however, one may note a number of grains growing and being consumed. While the time traces of the grain boundaries betray a certain amount of mobility, the crystallographic orientation of the grains do not seem to rotate significantly: the grey values of individual grains do not change with time. A finer observation of this last point is possible only on CIP images, as will be discussed in the last example.

We know from other work (Herwegh *et al.*, in press) that with respect to grain boundary migration, the HT–LS and IT–HS experiments differ in two aspects. Grain boundary migration is more predominant in the HT–LS than in the IT–HS experiment (compare fig. 8a and b in Herwegh *et al.*, in press), and the onset occurs earlier or more obviously with a steeper slope of the activity curve at a smaller shear strain. The first of these aspects should be seen as a difference in the opening angles of the diverging grain boundary time traces, with larger angles for the HT–LS than for the IT–HS time slices. However, as has been mentioned, opening angles are difficult to compare from one time slice to the next or from one experiment to the next. The second aspect should be seen as a difference in time coordinate where the parallel grain boundary time trace starts to diverge. However, on account of the repeated reorientation of the polarizers in the course of the HT–LS experiment, it is not possible to identify this point on the time slices of Fig. 5 with any reasonable precision.

HIGH TEMPERATURE–LOW STRAIN RATE EXPERIMENTS: *C*-AXIS ORIENTATION IMAGES (HT–LS COIS)

The time slices of the c-axis orientation images are taken along the same y-coordinates as those of the Pseudopol stack. Two slices are within the 'wallrock' at $y = 40$ and 280, and three slices within the shear zone at $y = 180$, 200 and 220 (see Fig. 6).

Orientation imaging

The colours of the orientation images represent unique directions of the c-axes as shown in the stereographic projection of the colour look-up table (CLUT) inserted in

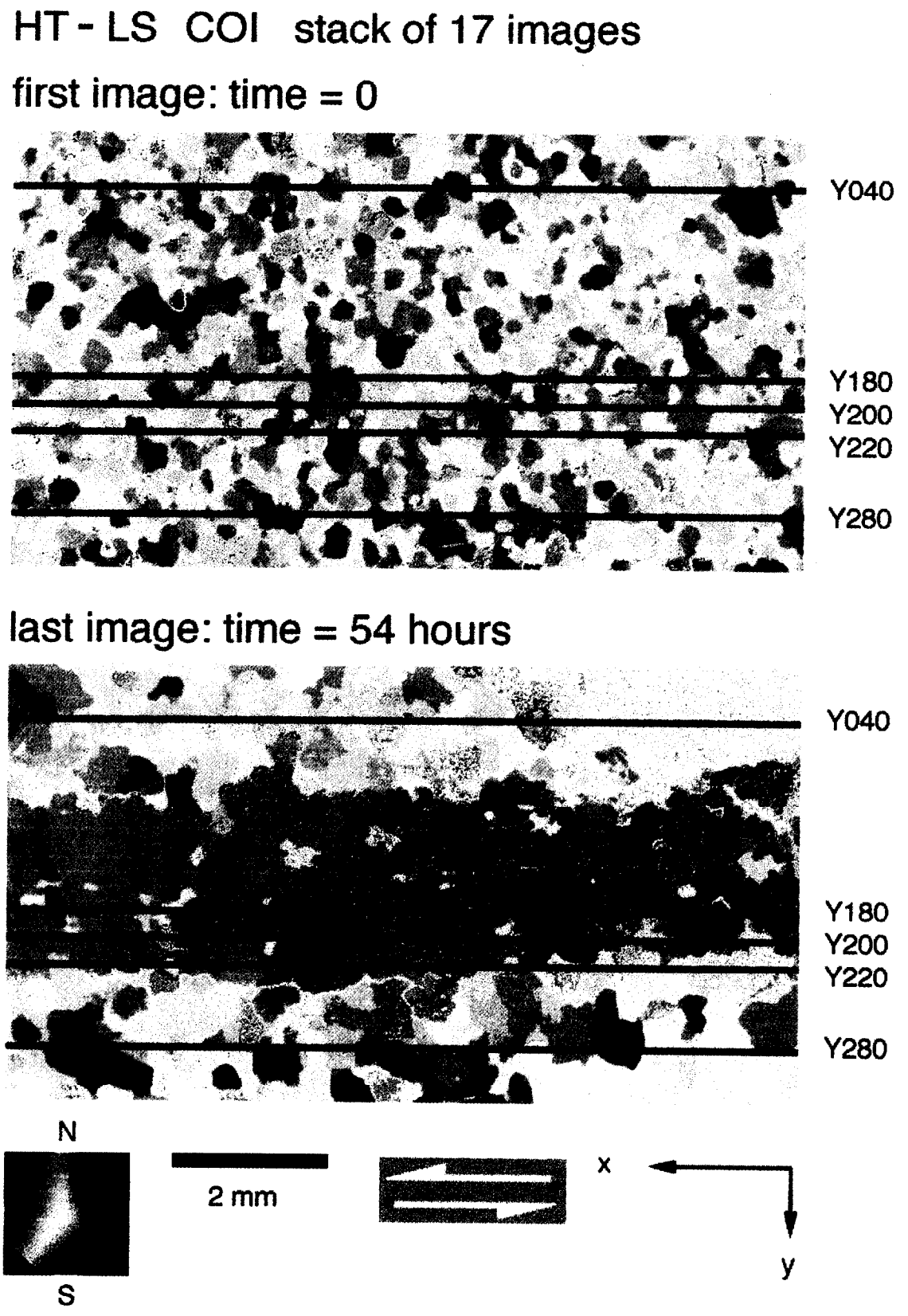

Fig. 6. First and last image of stack of HT–LS experiment on norcamphor (HT–LS = high temperature, low strain rate). Images are CIP calculated orientation images (see text). Traces for slicing at $y = 40$, 180, 200, 220 and 280 are indicated. For details of experimental conditions and polarizer orientation, consult Herwegh *et al.* (in press). Inset: stereographic representation of the colour look-up table (CLUT).

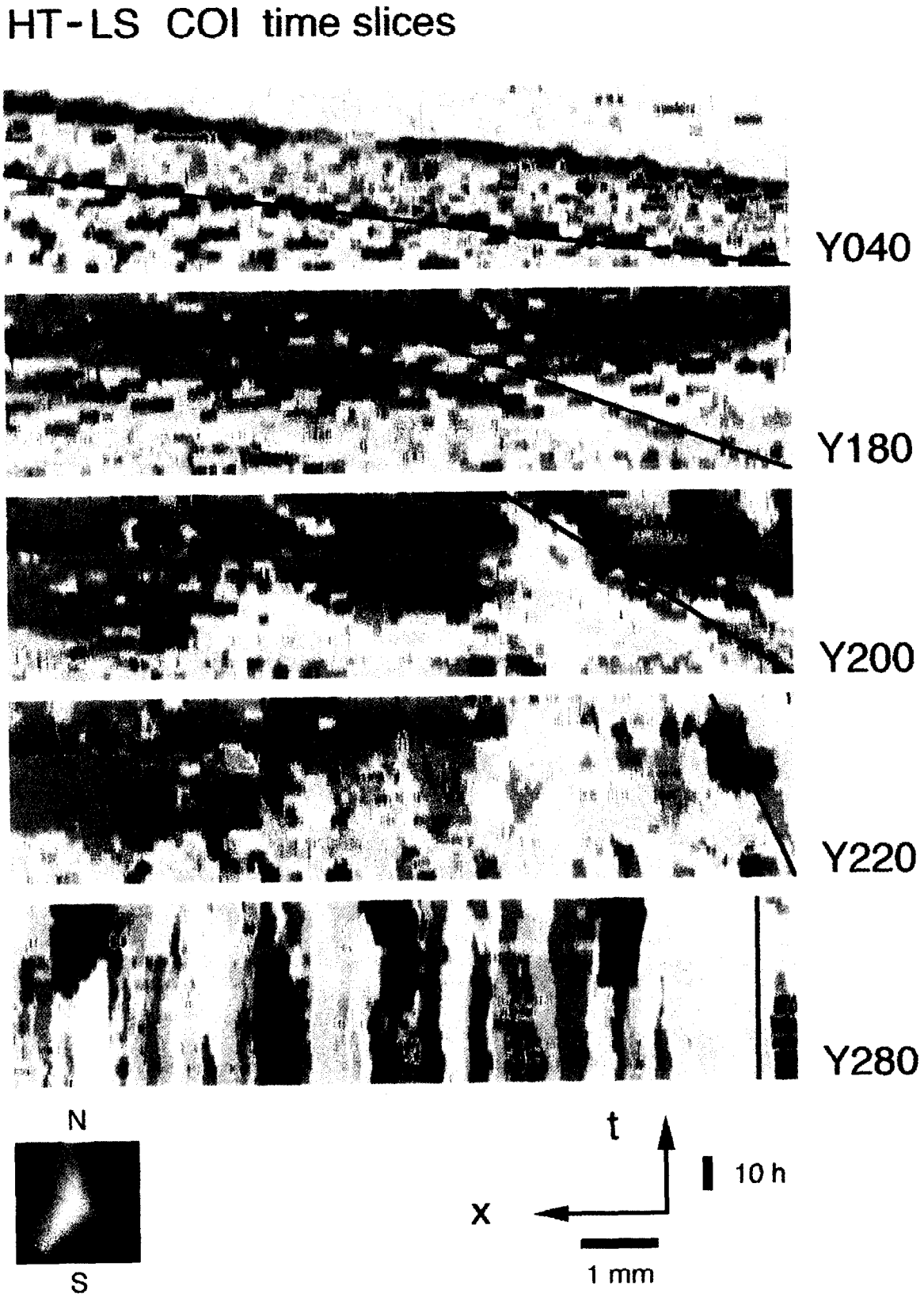

Fig. 7. Time slices of HT–LS-stack (Fig. 6). Slices at Y040 and Y280 are within the undeformed 'wallrock', slices Y180, Y200 and Y220 within the shear zone. Colours correspond to those of Fig. 6. The solid black lines on the time slices represent x-displacement rates. For time slice Y040 the x-displacement rate, v_x, was recalculated from the bulk behaviour of the 'wallrock material (see text for explanation). For time slices Y180, Y200 and Y220, the theoretical x-displacement rates, $v_x(y)$, were calculated from the x-displacement rate, v_x, of Y040 and the y-position of the time slice (see equation 4 in text). See text for explanation of red–cyan striping.

Fig. 6. Saturated colours represent c-axes orientations that are parallel to the x–y plane of the images; light colours represent c-axes that are normal to it, red and cyan (greenish–blue) denote N–S trending axes (N–S running parallel to the y-direction). The pinkish–greenish–yellowish hues of the first image of the time stack (Fig. 6, top) denote the almost random fabric of the initial material. There is in fact a weak preferred orientation of the c-axes which was introduced during the preparation of samples (see Herwegh *et al.*, in press).

In the course of deformation, the preponderance of N–S trending c-axes in the shear zone becomes visible as red and cyan colours. Note that red and cyan colours denote subparallel c-axis directions (see CLUT in Fig. 6), in other words the marked colour contrast over-emphasizes small directional variations. The horizontal red–cyan banding on the time slices is due to small angular differences from one time step to the next. Similar angular differences can be seen as lateral red–cyan transition on the individual x–y images of the stack (Fig. 6). It is possible to adapt (or scale) the visual contrast to the size of the directional differences by using so-called problem-adapted CLUTs whose colours wrap around the periphery of the stereonet (as in Herwegh *et al.*, in press, for example). Here, we will simply proceed by considering the red and cyan colours as being representatives of one and the same direction (N–S).

Microstructure of the 'wallrock'

In general, the colours of the grains in the 'wallrock' (Fig. 7, Y040 and Y280) remain the same throughout the experiment. Note a few green–purple stripes which are due to the same artefact as the red–cyan stripes of the shear zone discussed above. This means that the crystallographic orientation of the individual grains remains constant, i.e. on the grain scale, the lattices do not rotate.

In the stationary 'wallrock', grain growth is visible again (see description in the previous section). Upon first sight it appears as if there were a slight preference for the green and purple grains to grow. However, when comparing the colours of the first and the last image of the stack (Fig. 6) there is no significant shift of colours in the 'wallrock' regions. Thus, the overall texture of the undeformed material does not change.

Spatial arrangement of texture domains in shear zone

On the time slices Y180, Y200 and Y220 (Fig. 7), the most striking aspect is the replacement of the unsaturated colours of the initial fabric by the fully saturated red–cyan colours of the recrystallizing and growing grains. Starting from widely spaced sites of nucleation these grains grow and coalesce, forming ribbons, obliterating most of the initial orientations (Y200). It is not possible to confirm that the points of nucleation are periodically arranged within the shear zone. If they are, the periodicity of the recrystallizing domains is approximately 1/3 of the image width of the time slice. This corresponds to a periodicity wavelength of three times the width of the shear zone. Although there is an occasional reappearance of light coloured grains (c-axis normal to the x–y plane) within a red–cyan ribbon, the overall result after two thirds of the experiment (≈ 35 h; $g \approx 5$) is the formation of a continuous band of grains with nearly parallel N–S c-axis orientations.

At a few points on the time slices, the time boundary between the newly nucleated red–cyan grains and the obliterated old grains reveals an interesting contrast. The red–cyan regions nucleate or grow into the plane of the time slice with the c-axes already pointing N–S. On the grain scale, there is no rotation associated with growth and coalescence. Below this boundary, the light coloured initial grains appear to turn into white before they are consumed (nicely visible on Y200, Y220). In other words their c-axes appear to rotate towards the centre of the stereoplot. From the fact that the time boundary between old and new grains juxtaposes white and red–cyan grains, one might infer that the switch from old to new grain (by nucleation) occurs preferentially if the angle between the old and the new grain is close to 90°. This compares favourably with the stereoplots by Herwegh *et al.* (in press) which show a number of grains approaching the centre, i.e. an orientation normal to the plane of section, before they are consumed.

Lattice rotations

On time slices of orientation images, the change of colour parallel to the x-direction, i.e. for a fixed time t, denotes varying c-axis orientations in space; and abrupt variations indicate grain boundaries. Variations of colour along the v_x trace of individual grains, however, denote lattice rotations, i.e. change of orientation with time. In a few instances, the old, initial grains are not replaced by new ones; instead they rotate until they have achieved the favourable N–S c-axis orientation. On time slice Y220, just left of the middle, a transitions from orange to red may be seen, indicating a lattice rotation of 30–40° counterclockwise.

CONCLUSIONS

Applied to the x–y–t image stacks of *in situ* experiments, the technique of time slicing permits

(1) a check of the true bulk displacement of material in see-through experiments.

(2) the calculation of true bulk shear strain and shear strain rate.

(3) the recognition of grain growth.

(4) the recognition of the onset and dynamics of grain boundary migration.

(5) the recognition of lattice rotation on orientation images.

(6) the recognition of angular relations (misorientations) between host and new grain at the point of nucleation.

In comparison to other image processing methods for the analysis of microfabric development published by Bons *et al.* (1993) and Park (1994), time slicing has the merit of not requiring any time-consuming digitization of marker particles. In addition to providing precise estimates of bulk strain and bulk strain rate, it permits the detailed study of the temporal evolution of local phenomena along one spatial dimension. Time slicing is a technique whose major advantage is speed and ease of application. However, what we consider most important is the fact that it opens a new view on recorded films and time sequences of images.

Acknowledgements—We are indebted to Mark Jessell and Jin-Han Ree for constructive reviews. Support by the Swiss National Science Foundation (grants 21-36008.92, 20-42134.94 and 21-33814.92) is gratefully acknowledged.

REFERENCES

Bons, P. D., Jessell, M. W. and Passchier, C. W. (1993) The analysis of progressive deformation in rock analogues. *Journal of Structural Geology* **15**, 403–412.

Herwegh, M. (1996) Microfabric evolution in monomineralic mylonites: a rock analogue approach. Unpublished Ph.D. thesis, University of Berne.

Herwegh, M. and Handy, M. R. (1996) The evolution of high temperature mylonitic microfabrics: evidence from simple shearing of a quartz analogue (norcamphor). *Journal of Structural Geology* **18**, 689–710.

Herwegh, M., Handy, M. R. and Panozzo Heilbronner, R. (in press) Temperature and strain rate dependent microfabric evolution in monomineralic mylonite: evidence from in situ deformation of a rock analogue. *Tectonophysics*.

Jessell, M. W. (1986) Grain boundary migration and fabric development in experimentally deformed octachlorprpane. *Journal of Structural Geology* **8**, 527–542.

Panozzo Heilbronner, R. and Pauli, C. (1993) Integrated spatial and orientation analysis of quartz *c*-axes by computer-aided microscopy. *Journal of Structural Geology* **15**, 369–383.

Panozzo Heilbronner, R. and Pauli, C. (1994). Orientation and misorientation imaging: integration of microstructural and textural analysis. In *Textures of geological materials*, eds H. J. Bunge, S. Siegesmund, W. Skrotzki and K. Weber, pp. 147–164. DGM Informationsgesellschaft Verlag.

Panozzo Heilbronner, R. and Herwegh, M. (1995). Orientation imaging of see-through experiments using computer-integrated polarization microscopy (CIP). *Abstract Volume of the 12th Annual Meeting of the Swiss Tectonic Studies Group*, 22.

Park, Y. (1994) Microstructural evolution in crystal–melt systems. Unpublished Ph.D. thesis, State University of New York at Albany.

Rasband, W. (1995) NIH Image 1.57, public domain computer program. National Institutes of Health.

Warhol, A. (1963) Sleep, black and white film, 6 hours, with John Giorno.

Wells, H. G. (1895) *The Time Machine. New Centennial Edition*, ed. J. M. Everyman. Dent, London (1995).